AIMS Mathematics, 8(5): 10146−10159.
DOI: 10.3934/math.2023513
Received: 10 September 2022
Revised: 01 January 2023
Accepted: 18 January 2023
Published: 24 February 2023

http://www.aimspress.com/journal/Math

*Research article*

# Theoretical analysis of induced MHD Sutterby fluid flow with variable thermal conductivity and thermal slip over a stretching cylinder

**Nadeem Abbas[1], Wasfi Shatanawi[1,2,3,*], Taqi A. M. Shatnawi[3] and Fady Hasan[1]**

[1] Department of Mathematics and Sciences, College of Humanities and Sciences, Prince Sultan University, Riyadh 11586, Saudi Arabia
[2] Department of Medical Research, China Medical University Hospital, China Medical University, Taichung 40402, Taiwan
[3] Department of Mathematics, Faculty of Science, The Hashemite University, P.O. Box 330127, Zarqa 13133, Jordan

* **Correspondence:** Email: wshatanawi@psu.edu.sa; Tel: +962799724027.

**Abstract:** In the current analysis, steady incompressible Sutterby fluid flows over a stretching cylinder are studied. The influence of variable thermal conductivity is considered in the presence of thermal slip, Darcy resistance, and sponginess. The impact of the induced magnetic field is considered to analyze the results at the cylindrical surface. The governing equations are established as partial differential equations using the boundary layer approximation. Appropriate transformations are used to convert partial differential equations into ordinary differential equations. The numerical technique, namely (bvp4c), is applied to ordinary differential equations to develop the results. The numerical results, such as heat transfer rate and skin friction, are revealed by tabular form to demonstrate the physical impact of governing factors. The physical impact of governing factors on induced magnetic hydrodynamic, velocity, and temperature profiles is presented through various graphs. The velocity function deteriorated due to the augmentation of the Sutterby fluid parameter.

**Keywords:** induced magnetic field; Sutterby fluid; variable thermal conductivity; stretching cylinder; Darcy resistant
**Mathematics Subject Classification:** 76A05, 76W99, 80M25, 93A30

## 1. Introduction

The incompressible steady boundary layer flow of induced magnetic field Newtonian fluid over a stretching cylinder has achieved several claims in engineering and industrial areas. The induced magnetic field has achieved much attention from the authors due to several applications, including technological and scientific phenomena such as magneto-hydrodynamic boundary layer control technologies and magnetic hydrodynamic energy generator systems. Several applications in the real-life problem of magnetic hydrodynamics are as follows: heat exchanger processes, cancer treatment therapies, copper thinning wire, manufacturing power generators, etc. In the industrial problem, magnetohydrodynamics plays a critical role in controlling the cooling rate. Romig [1] discussed the impressions of magneto-electric fields on the electrically conducting fluid. The presented results have been developed experimentally. Tikhar et al. [2] studied the stability analysis of magnetic hydrodynamics at a stretching sheet. Numerical results have been developed. Phillips et al. [3] revealed the impression of the induced magnetic hydrodynamics. The induced magnetic hydrodynamics has been applied to gene transcription in different animals to analyze the effects of changes. Heine et al. [4] used the induced magnetic hydrodynamics of triple and double bond hydrocarbons, as well as cyclobutadiene and benzene. Ghosh et al. [5] debated free convection using the induced magnetic hydrodynamics. The Casson fluid model is considered to analyze the impact of the induced magnetic hydrodynamics on the stagnation region studied by Raju et al. [6]. The influence of homogeneous–heterogeneous reactions for Casson fluid is highlighted at the stretching surface. Al-Hanaya et al. [7] discussed the induced magnetic hydrodynamics for micropolar fluid using the SWCNT and MWCNT at a curved sheet. Khan et al. [8] deliberated the impact of Burger's nanofluid with a chemically interacting induced magnetic field on a stretchable nonlinear plate. Abbas et al. [9] debated the impact of a hybrid nanofluid in the presence of induced magnetic hydrodynamics in a stretched cylinder. Authors have recently industrialized the impact of induced magnetic hydrodynamics on various surfaces under a variety of assumptions (see Ref. [10,11]).

The study of boundary layer flow has proven preferable to Newtonian fluid in different physical, engineering, and industrial processes, such as gas turbines, the assembling of polymers, power generators, paper creation, glass fabrics, and wire drawing because of its applications in real life. It is one of the fluid models that extends the surprising performance of non-Newtonian fluids such as dilatant fluids and pseudo-plastic with properties that capture both the shear thickening and thinning properties of the flow. In particular, the shear thinning and shear thickening characteristics of high polymer aqueous solutions like carboxymethyl cellulose, methyl cellulose, and hydroxyethyl cellulose are reminiscent of Sutterby's model fluid. The use of diluted polymer solutions in industrial practice spans a wide variety of requests, including the spray application of agricultural chemicals, the reduction of drag in pipe flows, and the creation of household cleaning products. Analysts consider Sutterby liquid to be one of the most significant non-Newtonian liquids. Sutterby [12] was the first scientist to present the Satterby fluid model. Their nominal concentrations were 0.3, 0.5 and 0.7%. The viscosity data for each solution was filled with a generalized Newtonian viscosity model that accurately represented zero-shear viscosity. For each Natrosol solution in each conical segment, data on laminar flow rate and pressure drop are collected. Sutterby [13] was studied in two parts. Data on the viscosity of the polymer solution used in the convergent flow experiment. To fit these data, a new three-parameter viscosity model is used, which performs better than previous three-parameter models. The correspondence between velocity and pressure loss in laminar flow in a cylindrical tube were derived.

Tetsu et al. [14] discussed the non-Newtonian Sutterby fluid having natural convection. Batra and Eissa [15] studied the incompressible Sutterby fluid with heat transfer from free convection in the eccentric annulus. Akbar and Nadeem [16] highlighted the influence of peristaltic flow in the presence of Sutterby nanofluid. Hayat et al. [17] discussed the peristaltic flow numerically with the existence of radiative Sutterby nanofluid vertically. Ahmad et al. [18] debated the squeezing flow of Sutterby fluid with chemically radiative mixed convection at a stretching surface. Imran et al. [19] studied the influence of Sutterby fluid with chemically radiative mixed convection under the peristaltic mechanism. Sabir et al. [20] discussed the numerical results for Sutterby fluid flow having induced magnetic and radiation. The Sutterby fluid model is considered for the different flow assumptions at stretching surfaces by several authors, see Refs. [21,22].

Thermal conductivity has played an energetic role in the modern fluid dynamics at the stretching surface due to several applications of the real problem. Several authors have studied the constant variable thermal conductivity, which has been extensively studied in the literature. Due to that situation, the results of variable thermal conductivity using the perturbation method for convicting fin were developed by Krane [23]. Abu-Nada [24] developed the natural convection flow of nanomaterial fluid using temperature-dependent properties. Roslan et al. [25] deliberated the numerical results of variable thermal conductivity using the nanofluid model with Buoyancy-driven. Lin et al. [26] discussed the radiative Marangoni convection for non-Newtonian nanofluid flow using the variable thermal conductivity on an expansion plate. The numerical results have been developed for the phase flow Power-law fluid model. Gbadeyan et al. [27] analyzed the velocity slip and convicting heat of Casson nanomaterial fluid flow using the variable thermal conductivity. Maboob et al. [28] highlighted the temperature-dependent properties of Maxwell fluid flow under mass convection at a rotating disk. Ahmad et al. [29] deliberated the temperature-dependent properties of Maxwell nanofluid with chemical and bio-convective effects at stretching surfaces. Recently, few models of temperature-dependent properties of various fluid models on various stretching surfaces were studied by several authors, see Refs. [30−35].

We consider the steady flow of the incompressible induced magnetic field of Sutterby fluid over a nonlinear stretching cylinder. The slip impact is considered under the Darcy resistance and sponginess. The current analysis takes into consideration the temperature-dependent properties of liquids. Under the flow assumptions, the partial differential equations have been developed using the boundary layer approximations on the governing equations. Using appropriate transformations, differential equations can be transformed into dimensionless differential equations. A numerical approach is used to solve the dimensionless differential equation. The numerical results, such as Nusselt number and skin friction against the involving physical factors, are presented in tabular form. The results of velocity, temperature, and induced magnetic hydrodynamic profiles against physical factors, are presented through graphical form. The result of this study provides a new development method, which in turn will be very useful in the engineering and industrial fields.

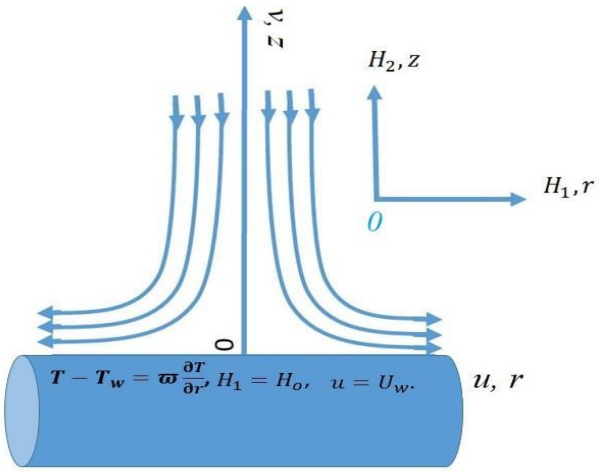


**Figure 1.** Flow pattern of Sutterby fluid over a circular cylinder.

## 2. Materials and methods

The incompressible steady flow of Sutterby fluid at a stretching cylinder is deliberated. The flow pattern of Sutterby fluid over a circular cylinder is presented in Figure 1. The temperature is an important factor that defines the thermo-physical properties of fluids. The thermal conductivity of the fluid is in a direct relationship with temperature, which has been experimentally proven. In 1950, Stanford University experimentally produced an electrically heated test panel that could determine heat transfer coefficients for specific causes. Temperature differences were typically less than $25\ F$. As a result, the effects of temperature dependence on fluid were so negligible that they could be considered constant properties. Variable thermal conductivity is revealed as $K(T) = k_\infty(1 + \epsilon\theta(\zeta))$, where $\epsilon$ is a very small parameter and constant thermal conductivity. If $\epsilon = 0$, it becomes constant thermal conductivity. Thermal slip is applied to the surface of the stretching cylinder. The impact of the induced magnetic hydrodynamics has also been publicized in the current analysis. $T_w$ is the wall temperature, $T_\infty$ is the ambient temperature, $r$ and $z$ are the radial axis and horizontal axis of the cylinder. $U_w$ is the wall stretching of the cylinder, $H_e$ free stream of induced magnetic field, $H_1$ and $H_2$ are the horizontal and radial induced magnetic field components of the cylinder. $u$ and $v$ are the velocity components along horizontal and radial directions. Boundary layer estimates are used to advance the differential equations according to the above assumptions. The differential equation system is as follows:

$$\frac{\partial u}{\partial r} + \frac{u}{r} + \frac{\partial v}{\partial z} = 0, \tag{1}$$

$$\frac{\partial H_1}{\partial r} + \frac{H_1}{r} + \frac{\partial H_2}{\partial z} = 0, \tag{2}$$

$$u\frac{\partial u}{\partial x}+v\frac{\partial v}{\partial r}-\frac{\mu_e}{4\pi\rho_f}\left(H_1\frac{\partial H_1}{\partial x}+H_2\frac{\partial H_1}{\partial r}\right) = \left(\frac{\upsilon_0}{2}\right)\frac{\partial^2 u}{\partial r^2}+\left(\frac{\upsilon_0}{2}\right)\frac{1}{r}\frac{\partial u}{\partial r}-\left(\frac{\upsilon_0 m a^2}{4}\right)\left(\frac{\partial u}{\partial r}\right)^2\frac{\partial^2 u}{\partial r^2}+\frac{R_z}{\rho_f}, \tag{3}$$

$$u\frac{\partial H_1}{\partial x}+v\frac{\partial H_1}{\partial r}-H_1\frac{\partial u}{\partial x}-H_2\frac{\partial u}{\partial r}=\eta_0\left(\frac{\partial^2 H_1}{\partial r^2}+\frac{1}{r}\frac{\partial H_1}{\partial r}\right), \tag{4}$$

$$u\frac{\partial T}{\partial x}+v\frac{\partial T}{\partial r}=\frac{1}{\rho c_p}\frac{1}{r}\frac{\partial}{\partial r}\left(K(T)r\frac{\partial T}{\partial r}\right), \tag{5}$$

with relevant boundary conditions are as following:

$$u=U_w,\quad v=0,\quad H_1=H_o,\quad H_2=0, T-T_w=\varpi\frac{\partial T}{\partial r},\ \ at\ \ r\to a, \qquad u\to 0,\quad H_1\to H_e,\quad T\to\ T_\infty,\ \ as\, r\to\infty. \tag{6}$$

Introducing the stream functions are:

$$u=\frac{1}{r}\frac{\partial\psi}{\partial r},\ \ v=\ -\frac{1}{r}\frac{\partial\psi}{\partial x},\ \ H_1=\frac{1}{r}\frac{\partial\psi_1}{\partial r},\ \ H_2=-\frac{1}{r}\frac{\partial\psi_1}{\partial x},\ \ \zeta=\frac{r^2-a^2}{2a}\sqrt{\frac{U_w}{\upsilon_f x}}, \qquad T=\ T_\infty+(T_w-\ T_\infty)\Theta, \tag{7}$$

where $\psi=\sqrt{2U_w\upsilon_f x}aF(\zeta)$ and $\psi_1=\ H_o a\sqrt{\frac{\upsilon_f}{U_w}}G(\zeta)$ are functions of stream velocity and magnetic field. The partial differential equations are changed to a dimensionless system as shown below using the appropriate transformation from above:

$$(1+2\zeta\gamma_1)F'''(\zeta)+2F''(\zeta)F(\zeta)-\left(F'(\zeta)\right)^2-\frac{\beta_1}{2}(1+2\zeta\gamma_1)^2\ \ (F''(\zeta))^2\,F'''(\zeta)+\frac{\lambda_1}{2}F'(\zeta)+\frac{1}{12}\beta_2\left(F''(\zeta)\right)^2F'^{(\zeta)}-\beta_0(G(\zeta)G''(\zeta)-G'(\zeta)G'(\zeta))=0, \tag{8}$$

$$\lambda_0(1+2\zeta\gamma_1)G'''(\zeta)+2\lambda_0\gamma_1G''(\zeta)-G''(\zeta)F(\zeta)+G(\zeta)F''(\zeta)=0, \tag{9}$$

$$\left(1+\epsilon\Theta(\zeta)\right)(1+2\zeta\gamma_1)\Theta''(\zeta)+\left(PrF(\zeta)+\gamma_1+\epsilon\gamma_1\Theta(\zeta)\right)\Theta'(\zeta)=0, \tag{10}$$

with the following boundary conditions:

$$F(0)=0,\ F'(0)=1,\ F'(\infty)=0,\ G(0)=0,\ G'(0)=0,\ G'(\infty)=1,\ \Theta(0)-1=\lambda_2\Theta'(0),\ \ \Theta(\infty)=0. \tag{11}$$

Here, ( $\lambda_2$) denotes to thermal slip, $\left(\gamma_1=\frac{1}{a}\sqrt{\frac{vl}{U_0}}\right)$ denotes to curvature parameter, $\left(\beta_1=\frac{\upsilon_0 m b^2 {U_0}^3 z^2}{l^3\upsilon_0}\right)$ denotes to Sutterby fluid parameter, $(\lambda_1=\frac{vl}{kU_0})$ denotes to sponginess parameter,

$\left(\beta_2 = \frac{\upsilon_0 mb^2 {U_0}^2 z^2}{l^2 \upsilon_0}\right)$ denotes to darcey resistant parameter, $(\beta_0)$ denotes to magnetic field parameter, $(\lambda_0)$ denotes to magnetic Prandtl number, $(\epsilon)$ denotes to variable thermal conductivity, and $(Pr = \frac{\upsilon_0}{\alpha})$ denotes the Prandtl number. The skin friction is defined as $C_f = \frac{\mu \tau_{rz}}{\rho {U_w}^2}{}_{,r=R}$ where $\tau_{rz}$ is the shear stress. The dimensionless heat transfer is Nusselt number $Nu_Z = \frac{q_w}{k(T_\infty - T_w)_{r=R}}$ and $q_w$ is heat flux. The dimensionless quantities of skin friction and Nusselt number are defined as:

$$C_f {R_e}^{1/2} = F''(0) - \frac{\beta_1}{4} F''(0)\left(4F'(0) + 4{\gamma_1}^2 F(0)\right)^2 - 4F(0)F'(0) + \lambda_1 F''(0)^2,$$

$$Nu_Z {R_e}^{-1/2} = \left(1 + \epsilon\Theta(0)\right)\Theta'(0).$$

## 3. Numerical method

The dimensionless system of differential equations (9−11) through boundary conditions (12) is elucidated through a numerical scheme. The numerical scheme, namely the fifth-order Runge–Kutta–Fehlberg method, is applied using the MATLAB software packages. The convergence criteria absolutely were taken as $10^{-6}$. The main selection of appropriate finite values of $\zeta_\infty$. The standard finite values of $\zeta_\infty$ is taken as $\zeta_7$ in boundary layer analysis, which satisfies our problem assumptions. The values of $\zeta_\infty = 7$ show that our results are corrected asymptotic values of the numerical solution. The procedure for a numerical solution is defined. The first step is transforming the higher-order dimensionless differential equation into first-order differential equations. The process of converting differential equations is defined as

$$F(\zeta) = S^*(1);\ F'(\zeta) = S^*(2);\ F''(\zeta) = S^*(3);\ \ F'''(\zeta) = S^*S^*1;$$

$$S^*S^*1 = \left(\frac{-1}{(1 + 2x\gamma_1) - \frac{\beta_1}{2}(1 + 2x\gamma)^2\, S^*(3)S^*(3)}\right)\Bigg(2S^*(1)S^*(3) - S^*(2)^2 - \frac{\beta_1}{2}(1 + 2\gamma_1\gamma)^2\ \left(\frac{\lambda_1}{2}S^*(2) + \frac{1}{12}\beta_2 S^*(3)S^*(3)S^*(2) + \beta_0\left(S^*(5)S^*(5) - S^*(4)S^*(6)\right)\right)\Bigg);$$

$$G(\zeta) = S^*(4);\ G'(\zeta) = S^*(5);\ \ G''(\zeta) = S^*(6);\ \ G'''(\zeta) = S^*S^*2;$$

$$S^*S^*2 = \left(\frac{-1}{(1 + 2x\gamma_1)\lambda_0}\right)\left(2\lambda_0\gamma_1 S^*(6) + S^*(4)S^*(3) - S^*(6)S^*(1)\right);$$

$$\Theta(\zeta) = S^*(7);\ \ \Theta'(\zeta) = S^*(8);\ \Theta''(\zeta) = S^*S^*3;$$

$$S^*S^*3 = \left(\frac{-1}{(1+2x\gamma_1)\left(1+\epsilon S^*(7)\right)}\right)\left(\left(PrS^*(1)+\gamma_1+\epsilon\gamma_1 S^*(7)\right)S^*(8)\right);$$

with boundary conditions are

$$S^*0(1);\ S^*0(2)-1;\ \ S^*inf(2);\ S^*0(4);\ S^*0(5);\ \ S^*inf(5)-1;\ \ S^*0(7)-1 \\ -\lambda_2\, S^*0(8);\ \ S^*inf(7).$$

## 4. Results and discussion

In this section, we will develop a mathematical model to solve differential equations (9−11) with the given boundaries. The differential equations are elucidated by a numerical procedure known as the bvp4c technique. The impacts of physical parameters are shown graphically as well as numerically in tabular form. Figures 2−6 explored the results of the stretching parameter, Darcy resistance parameter, Sutterby fluid parameter, magnetic hydrodynamic parameter, and sponginess parameter on the velocity function. Figure 2 shows the inspiration of the stretching parameter on the velocity. The velocity function revealed increasing behavior due to boosting values of the stretching factor. Figure 3 reveals the impression of the Darcy resistant parameter on the velocity function. The Darcy resistant parameter and velocity function have the same behavior of increasing. Figure 4 shows the effects of the Sutterby fluid parameter on the velocity function. Velocity function deteriorated by augmentation of Sutterby fluid factor. The distinction between the induced magnetic hydrodynamic parameter and velocity function is presented in Figure 5. It is seen that the velocity profile is enhanced by increasing the values of the induced magnetic hydrodynamic parameter. Figure 6 presents the impacts of the sponginess parameter on the velocity function. The velocity function declined due to sophisticated values of the sponginess parameter. Figures 7−10 depict the influence of the Prandtl number, thermal slip, stretching parameter, and variable thermal conductivity on the temperature function. Figure 7 revealed an impression of the Prandtl number on the temperature function. The curves of the temperature function declined due to greater values of the Prandtl number. Figure 8 depicts the impression of thermal slip on the temperature function. The temperature function declined due to the increase of thermal slip. The variation of a stretching parameter and temperature function is represented in Figure 9. The temperature function reveals boosting values due to increasing values of the stretching parameter. The variation of variable thermal conductivity and temperature function is depicted in Figure 10. The temperature function was boosted due to improving values of variable thermal conductivity. The inspiration of the magnetic Prandtl number and stretching parameter on the induced magnetic function which is reported in Figures 11 and 12. Figure 11 reported the impression of a magnetic Prandtl number on the induced magnetic profile. The induced magnetic function was enhanced due to boosting the values of magnetic Prandtl number. Figure 12 depicts the impact of stretching parameters on the induced magnetic function. The curves of the induced magnetic function and stretching parameter have the same behavior of increasing.

Table 1 reveals the impact of the curvature parameter ($\gamma_1$), Sutterby fluid parameter ($\beta_1$), sponginess parameter ($\lambda_1$), Darcy resistant parameter ($\beta_2$), magnetic field parameter ($\beta_0$), magnetic Prandtl number ($\lambda_0$), variable thermal conductivity ($\epsilon$), Prandtl number ($Pr$), and thermal slip ($\lambda_2$) on the friction factor and heat transfer. The values of curvature parameter ($\gamma_1$) is growing with declining the values of heat transfer and friction factor. The variation of Sutterby fluid parameter ($\beta_1$) with heat

transfer and friction factor is presented in Table 1. The friction factor values are boosted by increment of Sutterby fluid parameter ($\beta_1$) but is declining the heat transfer by improving the values of Sutterby fluid parameter ($\beta_1$). The variation of sponginess parameter ($\lambda_1$) with heat transfer and friction factor is presented in Table 1. The friction factor values are boosted by increment of sponginess parameter ($\lambda_1$) but is declining the heat transfer by improving the values of sponginess parameter ($\lambda_1$). Table 1 shows the variation of the Darcy resistance parameter ($\beta_2$) with heat transfer and friction factor. The heat transfer values are boosted by increment of Darcy resistant parameter ($\beta_2$) but is declining the friction factor by improving the values of Darcy resistant parameter ($\beta_2$). The variation of a magnetic field parameter ($\beta_0$) with heat transfer and friction factor is presented in Table 1. The heat transfer values are boosted by increment of magnetic field parameter ($\beta_0$)و but is declining the friction factor by improving the values of magnetic field parameter ($\beta_0$). Table 1 shows how the magnetic Prandtl number ($\lambda_0$) varies with heat transfer and friction factor. The friction factor values are boosted by increment the magnetic Prandtl number ($\lambda_0$), but is declining the heat transfer by improving the values of magnetic Prandtl number ($\lambda_0$). The variation of variable thermal conductivity ($\epsilon$) with heat transfer and friction factor is presented in Table 1. The friction factor values do not change as variable thermal conductivity ($\epsilon$) increases, but increasing variable thermal conductivity ($\epsilon$) decreases heat transfer. Table 1 shows how the Prandtl number ($Pr$) varies with heat transfer and friction factor. The friction factor values do not change by increment of Prandtl number ($Pr$), but is boosted the heat transfer by improving the values of Prandtl number ($Pr$). The distinction between thermal slip ($\lambda_2$), heat transfer, and friction factor is offered in Table 1. The values of the friction factor do not change by increment of thermal slip ($\lambda_2$), but the rate of heat transfer is declined by improving the values of thermal slip ($\lambda_2$).

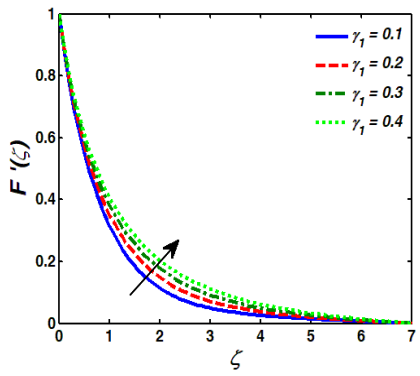


**Figure 2.** Impact of stretching factor on velocity.

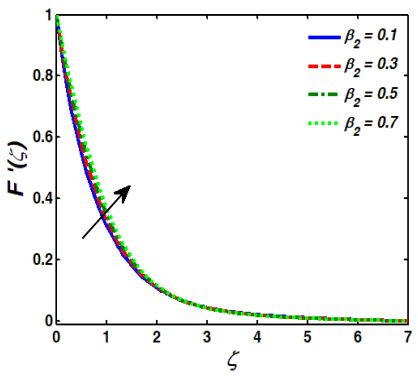


**Figure 3.** Impact of Darcy resistance factor on velocity.

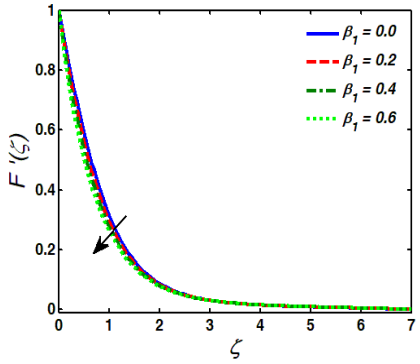


**Figure 4.** Impact of Sutterby fluid factor on velocity.

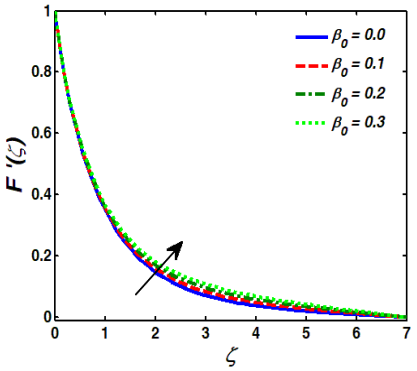


**Figure 5.** Impact of magnetic field factor on velocity.

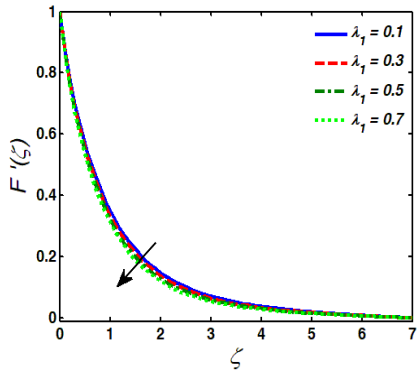


**Figure 6.** Impact of sponginess factor on velocity.

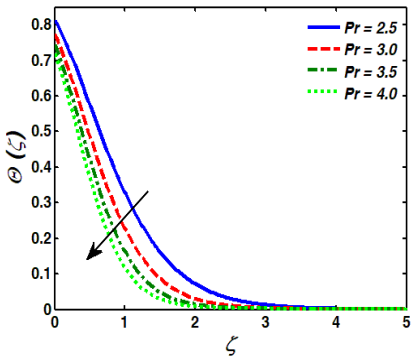


**Figure 7.** Impact of Prandtl number on temperature.

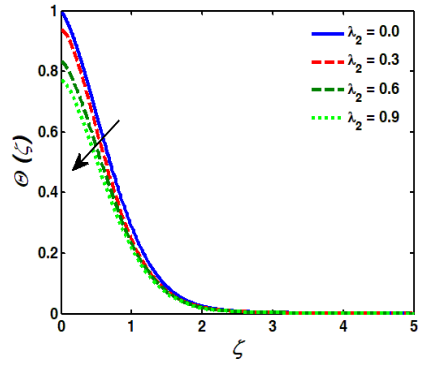


**Figure 8.** Impact of thermal slip on temperature.

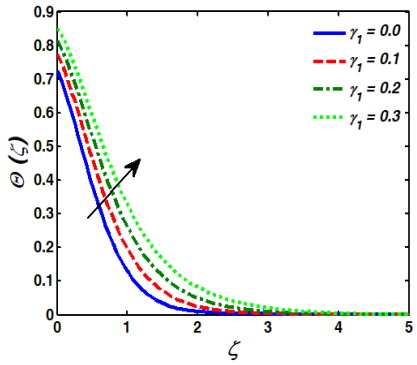


**Figure 9.** Impact of stretching factor on temperature.

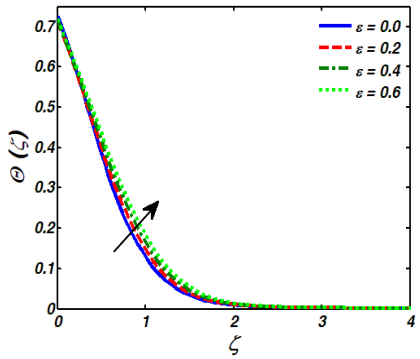


**Figure 10.** Impact of variable thermal conductivity on temperature.

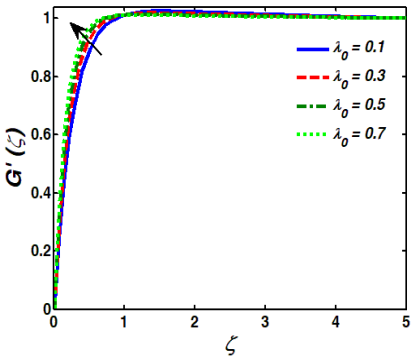


**Figure 11.** Impact of magnetic Prandtl number on induced magnetic field.

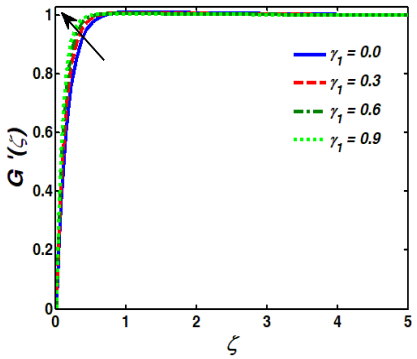


**Figure 12.** Impact of stretching factor on induced magnetic field.

**Table 1.** Numerical values of $-F''(0)$ and $-\Theta'(0)$ for various prominent factor.

| $\gamma_1$ | $\beta_1$ | $\lambda_1$ | $\beta_2$ | $\beta_0$ | $\lambda_0$ | $\epsilon$ | $Pr$ | $\lambda_2$ | $-F''(0)$ | $-\Theta'(0)$ |
|---|---|---|---|---|---|---|---|---|---|---|
| 0.0 | 0.3 | 0.4 | 0.1 | 0.3 | 0.5 | 0.4 | 1.5 | 0.2 | 1.2254380 | 0.65314076 |
| 0.2 | - | - | - | - | - | - | - | - | 1.2147324 | 0.55427329 |
| 0.4 | - | - | - | - | - | - | - | - | 1.1867793 | 0.51551367 |
| 0.6 | - | - | - | - | - | - | - | - | 1.1306222 | 0.49428495 |
| 0.4 | 0.1 | - | - | - | - | - | - | - | 1.1525344 | 0.51599928 |
| - | 0.3 | - | - | - | - | - | - | - | 1.1867793 | 0.51551367 |
| - | 0.5 | - | - | - | - | - | - | - | 1.2332398 | 0.51495428 |
| - | 0.7 | - | - | - | - | - | - | - | 1.3076062 | 0.51427441 |
| - | 0.3 | 0.2 | - | - | - | - | - | - | 1.1450581 | 0.51810286 |
| - | - | 0.4 | - | - | - | - | - | - | 1.1867793 | 0.51551367 |
| - | - | 0.6 | - | - | - | - | - | - | 1.2282558 | 0.51299404 |
| - | - | 0.8 | - | - | - | - | - | - | 1.2695100 | 0.51054327 |
| - | - | 0.4 | 0.1 | - | - | - | - | - | 1.1867793 | 0.51551367 |
| - | - | - | 0.2 | - | - | - | - | - | 1.1848012 | 0.51556424 |
| - | - | - | 0.3 | - | - | - | - | - | 1.1828305 | 0.51561477 |
| - | - | - | 0.4 | - | - | - | - | - | 1.1808670 | 0.51566527 |

*Continued on next page*

| $\gamma_1$ | $\beta_1$ | $\lambda_1$ | $\beta_2$ | $\beta_0$ | $\lambda_0$ | $\epsilon$ | $Pr$ | $\lambda_2$ | $-F''(0)$ | $-\Theta'(0)$ |
|---|---|---|---|---|---|---|---|---|---|---|
| - | - | - | 0.1 | 0.1 | - | - | - | - | 1.2355300 | 0.50768416 |
| - | - | - | - | 0.3 | - | - | - | - | 1.2113314 | 0.51156742 |
| - | - | - | - | 0.5 | - | - | - | - | 1.1867793 | 0.51551367 |
| - | - | - | - | 0.7 | - | - | - | - | 1.1618936 | 0.51951714 |
| - | - | - | - | 0.3 | 0.1 | - | - | - | 0.21245362 | 0.65030768 |
| - | - | - | - | - | 0.3 | - | - | - | 1.1300063 | 0.52425453 |
| - | - | - | - | - | 0.5 | - | - | - | 1.1867793 | 0.51551367 |
| - | - | - | - | - | 0.7 | - | - | - | 1.1982429 | 0.51368566 |
| - | - | - | - | - | 0.5 | 0.2 | - | - | 1.1867793 | 0.51923223 |
| - | - | - | - | - | - | 0.4 | - | - | 1.1867793 | 0.51551367 |
| - | - | - | - | - | - | 0.6 | - | - | 1.1867793 | 0.51193227 |
| - | - | - | - | - | - | 0.8 | - | - | 1.1867793 | 0.50854610 |
| - | - | - | - | - | - | 0.4 | 1.0 | - | 1.1867793 | 0.45237524 |
| - | - | - | - | - | - | - | 1.5 | - | 1.1867793 | 0.51551367 |
| - | - | - | - | - | - | - | 2.0 | - | 1.1867793 | 0.58023805 |
| - | - | - | - | - | - | - | 2.5 | - | 1.1867793 | 0.64528597 |
| - | - | - | - | - | - | - | 1.5 | 0.2 | 1.1867793 | 0.51551367 |
| - | - | - | - | - | - | - | - | 0.4 | 1.1867793 | 0.46789617 |
| - | - | - | - | - | - | - | - | 0.6 | 1.1867793 | 0.42825255 |
| - | - | - | - | - | - | - | - | 0.8 | 1.1867793 | 0.39475003 |

## 5. Conclusions

We considered the incompressible Sutterby fluid flow over a stretching cylinder. The influence of variable thermal conductivity is deliberated. To analyze the results at the cylindrical surface, the impact of the induced magnetic field is considered. Thermal slip impacts are considered in the presence of Darcy resistance and sponginess. The main results are presented as follows:

- The velocity function deteriorated due to higher values of the sponginess parameter. The Darcy resistant parameter and velocity function have the same behavior of increasing.
- The velocity function was augmented due to greater values of the magnetic field factor ($\beta_0$). The values of the Sutterby fluid parameter ($\beta_1$) were enhanced, which reduced the velocity profile. The skin friction values are boosted by increment of Sutterby fluid parameter ($\beta_1$) but is declining the rate of heat transfer by improving the values of Sutterby fluid parameter ($\beta_1$).
- The values of the sponginess parameter ($\lambda_1$) improved, which decayed the velocity profile. The heat transfer values are boosted by increment of Darcy resistant parameter ($\beta_2$) but is declining the skin friction by improving the values of Darcy resistant parameter ($\beta_2$).
- The heat transfer values are boosted by increment of magnetic field parameter ($\beta_0$), but skin friction is decreased by increasing the magnetic field parameter ($\beta_0$). The skin friction values are boosted by increment of magnetic Prandtl number ($\lambda_0$), but is declining the rate of heat transfer by improving the values of magnetic Prandtl number ($\lambda_0$).
- The curves of the induced magnetic function and stretching parameter have the same behaviour of increasing. The induced magnetic function was enhanced due to higher values of the magnetic Prandtl number.

## Acknowledgments

Authors would like to thank Prince Sultan University for their support through the TAS research lab.

## Conflict of interest

There is no conflict of interest.

## References

1. M. F. Romig, The influence of electric and magnetic fields on heat transfer to electrically conducting fluids, *Adv. Heat Transf.*, **1** (1964), 267−354. https://doi.org/10.1016/S0065-2717(08)70100-X
2. H. S. Takhar, M. Ali, A. S. Gupta, Stability of magnetohydrodynamic flow over a stretching sheet, In: *Liquid Metal Magnetohydrodynamics*, Dordrecht: Springer, 1989. https://doi.org/10.1007/978-94-009-0999-1_57
3. J. L. Phillips, W. Haggren, W. J. Thomas, T. Ishida-Jones, W. Ross Adey, Magnetic field-induced changes in specific gene transcription, *Biochim. Biophys. Acta Gene Struct. Expression*, **1132** (1992), 140−144. https://doi.org/10.1016/0167-4781(92)90004-J
4. T. Heine, R. Islas, G. Merino, σ and π contributions to the induced magnetic field: Indicators for the mobility of electrons in molecules, *J. Comput. Chem.*, **28** (2007), 302−309. https://doi.org/10.1002/jcc.20548
5. S. K. Ghosh, O. Anwar Bég, J. Zueco, Hydromagnetic free convection flow with induced magnetic field effects, *Meccanica*, **45** (2010), 175−185. https://doi.org/10.1007/s11012-009-9235-x
6. C. S. K. Raju, N. Sandeep, S. Saleem, Effects of induced magnetic field and homogeneous-heterogeneous reactions on stagnation flow of a Casson fluid, *Eng. Sci. Technol. Int. J.*, **19** (2016), 875−887. https://doi.org/10.1016/j.jestch.2015.12.004
7. A. M. Al-Hanaya, F. Sajid, N. Abbas, S. Nadeem, Effect of SWCNT and MWCNT on the flow of micropolar hybrid nanofluid over a curved stretching surface with induced magnetic field, *Sci. Rep.*, **10** (2020), 8488. https://doi.org/10.1038/s41598-020-65278-5
8. M. N. Khan, S. Nadeem, N. Abbas, A. M. Zidan, Heat and mass transfer investigation of a chemically reactive Burgers nanofluid with an induced magnetic field over an exponentially stretching surface, *P. I. Mech. Eng. E-J. Pro.*, **235** (2021), 2189−2200. https://doi.org/10.1177/09544089211034941
9. N. Abbas, S. Nadeem, A. Saleem, M. Y. Malik, A. Issakhov, F. M. Alharbi, Models base study of inclined MHD of hybrid nanofluid flow over nonlinear stretching cylinder, *Chin. J. Phys.*, **69** (2021), 109−117. https://doi.org/10.1016/j.cjph.2020.11.019
10. M. I. Anwar, H. Firdous, A. A. Zubaidi, N. Abbas, S. Nadeem, Computational analysis of induced magnetohydrodynamic non-Newtonian nanofluid flow over nonlinear stretching sheet, *Prog. React. Kinet.*, **47** (2022). https://doi.org/10.1177/14686783211072712

11. N. Abbas, S. Nadeem, M. N. Khan, Numerical analysis of unsteady magnetized micropolar fluid flow over a curved surface, *J. Therm. Anal. Calorim.*, **147** (2022), 6449−6459. https://doi.org/10.1007/s10973-021-10913-0
12. J. L. Sutterby, Laminar converging flow of dilute polymer solutions in conical sections. II, *Trans. Soc. Rheol.*, **9** (1965), 227−241. https://doi.org/10.1122/1.549024
13. J. L. Sutterby, Laminar converging flow of dilute polymer solutions in conical sections: Part I. Viscosity data, new viscosity model, tube flow solution, *AIChE J.*, **12** (1966), 63−68. https://doi.org/10.1002/aic.690120114
14. T. Fujii, O. Miyatake, M. Fujii, H. Tanaka, K. Murakami, Natural convective heat transfer from a vertical isothermal surface to a non-Newtonian Sutterby fluid, *Int. J. Heat Mass Transf.*, **16** (1973), 2177−2187. https://doi.org/10.1016/0017-9310(73)90005-7
15. R. L. Batra, M. Eissa, Laminar forced convection heat transfer of a Sutterby model fluid in an eccentric annulus, *Mech. Res. Commun.*, **21** (1994), 147−152. https://doi.org/10.1016/0093-6413(94)90087-6
16. N. S. Akbar, S. Nadeem, Nano Sutterby fluid model for the peristaltic flow in small intestines, *J. Comput. Theor. Nanosci.*, **10** (2013), 2491−2499. https://doi.org/10.1166/jctn.2013.3238
17. T. Hayat, H. Zahir, M. Mustafa, A. Alsaedi, Peristaltic flow of Sutterby fluid in a vertical channel with radiative heat transfer and compliant walls: A numerical study, *Results Phys.*, **6** (2016), 805−810. https://doi.org/10.1016/j.rinp.2016.10.015
18. S. Ahmad, M. Farooq, M. Javed, A. Anjum, Double stratification effects in chemically reactive squeezed Sutterby fluid flow with thermal radiation and mixed convection, *Results Phys.*, **8** (2018), 1250−1259. https://doi.org/10.1016/j.rinp.2018.01.043
19. N. Imran, M. Javed, M. Sohail, P. Thounthong, Z. Abdelmalek, Theoretical exploration of thermal transportation with chemical reactions for sutterby fluid model obeying peristaltic mechanism, *J. Mater. Res. Technol.*, **9** (2020), 7449−7459. https://doi.org/10.1016/j.jmrt.2020.04.071
20. Z. Sabir, A. Imran, M. Umar, M. Zeb, M. Shoaib, M. A. Z. Raja, A numerical approach for 2-D Sutterby fluid-flow bounded at a stagnation point with an inclined magnetic field and thermal radiation impacts, *Therm. Sci.*, **25** (2021), 1975−1987. https://doi.org/10.2298/TSCI191207186S
21. S. Abdal, I. Siddique, S. Afzal, S. Sharifi, M. Salimi, A. Ahmadian, An analysis for variable physical properties involved in the nano-biofilm transportation of Sutterby fluid across shrinking/stretching surface, *Nanomaterials*, **12** (2022), 599. https://doi.org/10.3390/nano12040599
22. S. Bilal, I. A. Shah, A. Akgül, M. T. Tekin, T. Botmart, E. S. Yousef, et al., A comprehensive mathematical structuring of magnetically effected Sutterby fluid flow immersed in dually stratified medium under boundary layer approximations over a linearly stretched surface, *Alex. Eng. J.*, **61** (2022), 11889−11898. https://doi.org/10.1016/j.aej.2022.05.044
23. R. J. Krane, Discussion:"Perturbation solution for convecting fin with variable thermal conductivity", *J. Heat Transfer.*, **98** (1976), 685. https://doi.org/10.1115/1.3450625
24. E. Abu-Nada, Effects of variable viscosity and thermal conductivity of $Al_2O_3$-water nanofluid on heat transfer enhancement in natural convection, *Int. J. Heat Fluid Flow*, **30** (2009), 679−690. https://doi.org/10.1016/j.ijheatfluidflow.2009.02.003
25. R. Roslan, H. Saleh, I. Hashim, Buoyancy-driven heat transfer in nanofluid-filled trapezoidal enclosure with variable thermal conductivity and viscosity, *Numer. Heat Transf. A*, **60** (2011), 867−882. https://doi.org/10.1080/10407782.2011.616778

26. Y. H. Lin, L. C. Zheng, X. X. Zhang, Radiation effects on Marangoni convection flow and heat transfer in pseudo-plastic non-Newtonian nanofluids with variable thermal conductivity, *Int. J. Heat Mass Transf.*, **77** (2014), 708−716. https://doi.org/10.1016/j.ijheatmasstransfer.2014.06.028
27. J. A. Gbadeyan, E. O. Titiloye, A. T. Adeosun, Effect of variable thermal conductivity and viscosity on Casson nanofluid flow with convective heating and velocity slip, *Heliyon*, **6** (2020), e03076. https://doi.org/10.1016/j.heliyon.2019.e03076
28. F. Mabood, A. Rauf, B. C. Prasannakumara, M. Izadi, S. A. Shehzad, Impacts of Stefan blowing and mass convention on flow of Maxwell nanofluid of variable thermal conductivity about a rotating disk, *Chin. J. Phys.*, **71** (2021), 260−272. https://doi.org/10.1016/j.cjph.2021.03.003
29. S. Ahmad, M. Naveed Khan, S. Nadeem, Unsteady three dimensional bioconvective flow of Maxwell nanofluid over an exponentially stretching sheet with variable thermal conductivity and chemical reaction, *Int. J. Ambient Energy*, **43** (2022), 6542−6552. https://doi.org/10.1080/01430750.2022.2029765
30. M. Ramzan, N. Shahmir, H. A. S. Ghazwani, Stefan blowing impact on bioconvective Maxwell nanofluid flow over an exponentially stretching cylinder with variable thermal conductivity, *Wave Random Complex*, 2022. https://doi.org/10.1080/17455030.2022.2102269
31. H. Waqas, A. Kafait, M. Alghamdi, T. Muhammad, A. S. Alshomrani, Thermo-bioconvectional transport of magneto-Casson nanofluid over a wedge containing motile microorganisms and variable thermal conductivity, *Alex. Eng. J.*, **61** (2022), 2444−2454. https://doi.org/10.1016/j.aej.2021.07.006
32. D. O. Soumya, B. J. Gireesha, P. Venkatesh, Planar Couette flow of power law nanofluid with chemical reaction, nanoparticle injection and variable thermal conductivity, *Proc. Inst. Mech. Eng. C-J. Mech. Eng. Sci.*, **236** (2022), 5257−5268. https://doi.org/10.1177/09544062211059071
33. Y. Nawaz, M. S. Arif, K. Abodayeh, M. Bibi, Finite element method for non-newtonian radiative Maxwell nanofluid flow under the influence of heat and mass transfer, *Energies*, **15** (2022), 4713. https://doi.org/10.3390/en15134713
34. Y. Nawaz, M. S. Arif, K. Abodayeh, A third-order two-stage numerical scheme for fractional Stokes problems: A comparative computational study, *J. Comput. Nonlinear Dynam.*, **17** (2022), 101004. https://doi.org/10.1115/1.4054800
35. Y. Nawaz, M. S. Arif, K. Abodayeh, Predictor-Corrector scheme for electrical Magnetohydrodynamic (MHD) Casson nanofluid flow: A computational study, *Appl. Sci.*, **13** (2023), 1209. https://doi.org/10.3390/app13021209